Nonmodel-based framework for rapid seismic risk and loss assessment of instrumented steel buildings

Seong-Hoon Hwang[a], Dimitrios G. Lignos[a,*]

[a]*Department of Architecture, Civil and Environmental Engineering, Swiss Federal Institute of Technology, Lausanne (EPFL), Switzerland*

Abstract

This paper proposes a nonmodel-based framework for estimating story-based engineering demand parameters (EDPs) in instrumented steel frame buildings with steel moment-resisting frames (MRFs). The proposed framework utilizes a wavelet-based damage-sensitive feature and basic building geometric information to infer the building damage state at a given seismic intensity. The story-based EDPs are predicted with a reasonable accuracy compared to those predicted from rigorous nonlinear response history analyses that typically require the explicit use of a nonlinear building model. The efficiency of the proposed framework is demonstrated through a number of illustrative examples including actual instrumented steel frame buildings that experienced the 1994 Northridge earthquake in Los Angeles. It is shown that if the building content is known the proposed framework can facilitate building-specific seismic risk and loss assessment within minutes after an earthquake provided that the recorded floor absolute acceleration histories at discrete locations along the height of the building are accessible. The nonmodel-based framework is also extended at the city-scale through the development of generalized earthquake-induced damage and loss maps for the same earthquake event. The same framework can facilitate the decision-making for effective pre-disaster measures for earthquake disaster risk management of building assets.

Keywords: Rapid seismic risk assessment, Instrumented steel buildings, Wavelet analysis, Earthquake-induced loss assessment, Generalized loss map, City-scale simulation, Disaster-risk management

1. Introduction

City-scale safety assessment in the aftermath of an earthquake is a challenging problem with vast socio-economic consequences. In that sense, visual inspections [1–4] have been historically employed. Such inspections may take months to complete and therefore earthquake-induced losses due to downtime can be considerable [1–4]. A number of researchers have utilized model-based approaches for the earthquake-induced structural and non-structural damage assessment (e.g., [5–11]). Although such approaches predict reasonably well story-based engineering demand parameters (EDPs) they typically require the explicit use of nonlinear building models and subsequently an appreciable

*Corresponding author
Email addresses: seong-hoon.hwang@epfl.ch (Seong-Hoon Hwang), dimitrios.lignos@epfl.ch (Dimitrios G. Lignos)

time investment for the model validation. Therefore, such approaches cannot be used in the context of community resilience in which a rapid seismic risk assessment of building assets is necessary.

Vibration-based condition assessment [12–18] is an interesting alternative compared to *model-based* approaches conditioned that ambient vibration monitoring data is available and/or a seismic instrumentation program has been already established within the earthquake-affected region [19–21]. A challenge in this case could be that a densely arrayed sensing system may be required [22, 23]. Noh et al. [17, 18] proposed EDP indicators for *nonmodel-based* seismic vulnerability assessment of steel frame buildings by observing the changes in wavelet energies at a particular scale over time. In a more recent study, Hwang and Lignos [24] demonstrated that the wavelet-based damage-sensitive features (DSFs) can facilitate the seismic vulnerability assessment of buildings with fairly low instrumentation density. However, the challenge to establish the relationship between the wavelet energy shifting at a particular building frequency and the story-based building EDP estimates still remains. These EDPs are essential to facilitate earthquake-induced risk and loss assessment at a given seismic intensity.

In this paper, we propose a framework that facilitates the rapid seismic risk and loss assessment of instrumented steel frame buildings. The proposed framework is based on a nonmodel-based approach that combines concepts from structural health monitoring and performance-based earthquake engineering. The efficiency of the proposed framework is evaluated in three parts. The first part illustrates comparisons between the proposed framework and computationally intensive state-of-the-art approaches in predicting story-based building EDPs at a given seismic intensity. The second part utilizes the proposed framework to conduct a rapid seismic risk and loss assessment of an instrumented steel frame building that experienced the 1994 Northridge earthquake. The final part of the paper describes how the proposed framework can be extended at a city-scale in order to facilitate regional earthquake-induced loss assessment for emergency-response operations in the aftermath of an earthquake and pre-disaster measures for earthquake risk management.

2. Proposed framework for performance-based rapid assessment of steel frame buildings

This section presents a framework for performance-based rapid seismic vulnerability assessment of instrumented steel frame buildings. The emphasis is currently on steel frame buildings with MRFs as their lateral load-resisting system. Figure 1 illustrates schematically the main components of the proposed framework. The first step involves the collection of basic information from the instrumented building of interest including the number of stories and the building height. In terms of recorded data, the absolute acceleration at the roof of the building is only required. Referring to Figure 1, the proposed framework requires the identification of the dynamic properties of the instrumented building inferred to its undamaged state. This is further elaborated in Section 2.1.

Once the dynamic properties of the instrumented building are known, a refined wavelet-based DSF [17, 24] is employed. The wavelet-based DSF is extracted from the measured absolute acceleration at the building roof. This is discussed in detail in Section 2.2. Referring to Figure 1, the third component of the proposed framework includes the

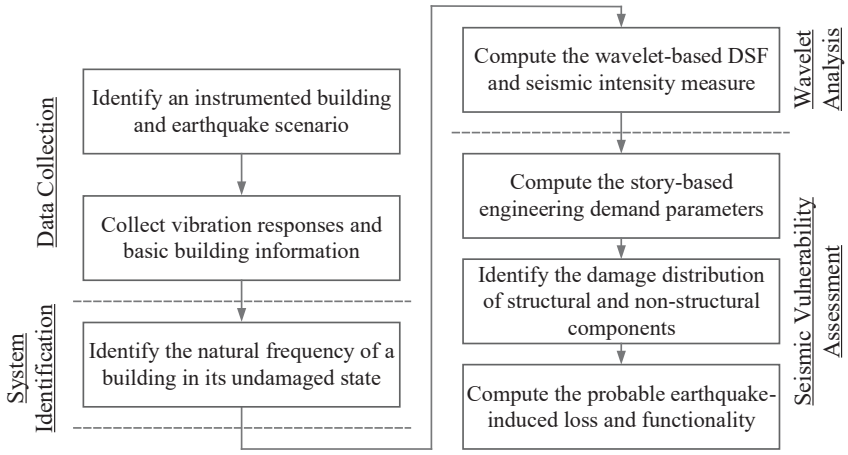

Figure 1: Flowchart of the proposed framework for rapid seismic risk and loss assessment of instrumented steel frame buildings.

mapping of the computed DSFs with story-based EDPs along the height of the instrumented building. This mapping is achieved through multivariate regression equations that relate the wavelet-based DSFs and basic geometric building characteristics with story-based EDPs at a given seismic intensity (see Section 2.3). Finally, the earthquake-induced economic losses are computed. Referring to Figure 1, depending on the density of the instrumented buildings within an earthquake-prone region a generalized loss map can be generated through the use of the geographic information system (GIS). The subsequent sections provide specific details of the main components of the proposed framework for seismic risk and loss assessment of instrumented steel frame buildings.

2.1. System identification

To compute the wavelet-based DSFs, the first natural frequency, f_1 of the undamaged state of a building is required. For this purpose, the use of ambient vibrations obtained before the earthquake occurs is preferred if available. Output-only system identification methods can be utilized because of the absence of a measured input excitation [13]. Otherwise, the last portion of the measured vibration recorded during a strong motion is considered as the vibration response of the undamaged instrumented building. The last portion is determined as the number of data points to provide best frequency resolution (0.097 Hz) for distinctive peaks in the power spectrum density diagram (PSD) estimation by applying a fast Fourier transform with a 1024-point Hann window [25]. In this paper, the autoregressive with exogenous term (ARX) method [14] is utilized for this purpose. The ARX model uses least squares to estimate the dynamic properties of a multi-degree-of-freedom (MDF) system from recorded absolute acceleration data in the discrete time domain. This model is mathematically defined as follows,

$$\sum_{i=0}^{M} \mathbf{A}_i \mathbf{y}(n-i) = \sum_{i=0}^{M} \mathbf{B}_i \mathbf{x}(n-i) + \mathbf{e}(n) \tag{1}$$

in which M is the model order of the ARX model; $\mathbf{x}(n)$ and $\mathbf{y}(n)$ are the p-dimensional input and q-dimensional output vectors, respectively; $\mathbf{e}(n)$ is the residue error vector; and $\mathbf{A}_i$ and $\mathbf{B}_i$ are $p \times p$ and $q \times p$ coefficient matrices of the autoregressive (AR) polynomial and exogenous (X) input. The model in Eq. (1) may be re-written as follows,

$$\mathbf{y}(n) = -\sum_{i=1}^{M} \mathbf{A}_i \mathbf{y}(n-i) + \sum_{i=0}^{M} \mathbf{B}_i \mathbf{x}(n-i) + \mathbf{e}(n) = \mathbf{\Phi}^T(n) \cdot \mathbf{\Theta} + \mathbf{e}(n) \tag{2}$$

in which

$$\mathbf{\Phi}^T(n) = \begin{bmatrix} -\mathbf{y}(n-1) & \cdots & -\mathbf{y}(n-M) & \mathbf{x}(n-1) & \cdots & \mathbf{x}(n-M) \end{bmatrix} \tag{3}$$

$$\mathbf{\Theta} = \begin{bmatrix} \mathbf{A}_1 & \cdots & \mathbf{A}_M & \mathbf{B}_1 & \cdots & \mathbf{B}_M \end{bmatrix}^{\mathrm{T}} \tag{4}$$

The parameter matrix, $\mathbf{\Theta}$ can be estimated based on the least square method as follows,

$$\arg\min_{\mathbf{\Theta}} J(\mathbf{\Theta}) = \arg\min_{\mathbf{\Theta}} \left\| \mathbf{y}(n) - \mathbf{\Phi}^T(n) \cdot \mathbf{\Theta} \right\|^2 \tag{5}$$

The AR coefficient and X input matrices are used to formulate the system matrix of equations. The dynamic properties of a MDF system are estimated by eigenvalue decomposition for the system matrix [14].

Due to random noise, it is common that spurious modes are induced [12, 14]. In this case, a stable mode is estimated by changing the ARX model order. A stabilization diagram [12, 14] is typically used for this purpose. From this diagram, stabilization occurs when the relative differences of the dynamic properties identified using two different model orders are not more than 5%, 10%, and 5% for the natural frequencies, the damping ratios, and the modal assurance criterion (MAC) of mode shapes [12] (i.e., convergence thresholds), respectively. Figure 2 illustrates the stabilization diagram for the y loading direction of a 4-story steel frame building with moment-resisting frames (MRFs) tested at the E-Defense facility [26, 27] estimated based on the single-input/three-output ARX method. Referring to Figure 2, a relatively solid vertical line represents true modes. Moreover, the circled symbols represent the values that were converged to the thresholds for the frequency, MAC and damping ratio.

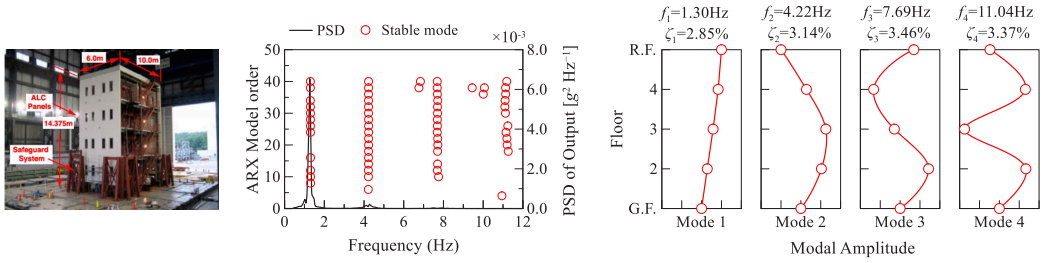

(a) overview of test setup (b) stabilization diagram (c) identified dynamic properties

Figure 2: Stabilization diagram of the y loading direction of the 4-story steel frame building with MRFs tested at E-Defense facility.

2.2. *Wavelet-based damage-sensitive features*

In order to develop an approximate method for rapid earthquake vulnerability assessment of steel frame buildings with MRFs, a nonmodel-based approach is employed. In particular, wavelet-based DSFs are utilized as proposed in [17]. The wavelet-based DSFs are computed based on the absolute acceleration response history recorded at the building roof. The DSFs are then interpreted as story-based EDP indicators by monitoring the change in wavelet-based DSFs at a given seismic intensity. This section briefly describes the theoretical background of the wavelet-based DSF that is utilized in this paper. Given a scale parameter $a > 0$, and time shift parameter b, the continuous wavelet transform can be mathematically described as follows,

$$C(a,b) = \int_{-\infty}^{\infty} f(t) \frac{1}{\sqrt{a}} \psi^* \left(\frac{t-b}{a} \right) \mathrm{d}t \tag{6}$$

in which $f(t)$ is the response history data (i.e., the absolute acceleration time history in this paper); $\psi(t)$ is the mother wavelet function (the Morlet wavelet basis function [28] is used as a mother wavelet due to its resemblance to earthquake pulse); and * is the complex conjugate. A set of basis functions, which are termed as daughter wavelets, is established by continuously dilating and translating the mother wavelet function, $\psi(t)$. The continuous wavelet transform coefficients, $C(a,b)$ are then obtained by convoluting the basis functions and recorded absolute acceleration history data, $f(t)$ at the building roof.

Noh et al. [17] introduced the wavelet-based DSFs as structural damage indicators, which are defined as the ratio of the wavelet energy at the first-mode natural frequency of the building over time to the total wavelet energy. Hwang and Lignos [24] refined the wavelet-based DSF for cases that higher mode contributions become considerable. Therefore, the wavelet-based DSFs as proposed in [24] are utilized as follows,

$$DSF = 1 - \frac{\sum_{i=1}^{3} E_{\mathrm{scale}(f_i)}}{E_{\mathrm{tot}}} \tag{7}$$

in which $E_{\mathrm{scale}(f_i)}$ is the wavelet energy at a scale corresponding to the *i*th natural frequency of the building under consideration. Referring to Eq. (7), the DSF values represent how the distribution of vibration energies at the natural frequencies of a building changes while the structural damage progresses. Therefore, the DSF values range between 0 (representing no structural damage) and 1 (representing severe structural damage) as suggested in [17]. The DSF is a more rational damage indicator than the peak absolute acceleration at the building roof that more-of-less saturates once the building enters into the inelastic regime. The wavelet energy $E_{\mathrm{scale}(f_i)}$ shows how the vibration energy of the acceleration response data is distributed over time given at a particular scale (i.e., the scale corresponding to *i*th natural frequency). By assuming that the natural frequencies of the building are well separated, the second- and third-mode natural frequencies are approximated at $3f_1$ and $5f_1$, respectively [29]. The wavelet energy, $E_{\mathrm{scale}(f_i)}$ can then be computed as follows,

$$E_{\text{scale}(f_i)} = \sum_{b=1}^{K} \left| C\left(f_i, b \times \Delta t\right) \right|^2 \tag{8}$$

Referring to Eq. (7), the total wavelet energy, E_{tot} of the recorded absolute acceleration response history is defined as follows,

$$E_{\text{tot}} = \sum_{i=1}^{3} E_{\text{scale}(f_i)} + E_{\text{scale}(0.5\times f_1)} + E_{\text{scale}(2\times f_1)} + E_{\text{scale}(4.5\times f_1)} \tag{9}$$

Hwang and Lignos [24] conducted further validations on the potential use of wavelet-based DSFs for structural damage identification based on full-scale shake table experiments on steel frame buildings with steel MRFs and concentrically braced frames (CBFs). They found that when we consider the wavelet energies at scales that correspond to the first three natural frequencies of the respective building is typically enough to capture the higher mode effects on the building seismic response. The extra energy terms at $0.5/2/4.5 \times f_1$ in Eq. (9) are explicitly considered in order to capture a wavelet energy shift due to decrease in the first three natural frequencies of the respective building due to the onset of structural damage. Hwang and Lignos [24] also found that the mapping of a DSF value to the maximum EDP across all stories of a building is possible at a given seismic intensity when the absolute floor acceleration history at the roof of a building is recorded. This is illustrated in Figure 3 for the 4-story steel frame building with MRFs that was tested at the E-Defense shake table through collapse [26, 27]. The building was subjected to the JR Takatori ground motion from the 1995 Hygoken-Nanbu earthquake. Referring to Figure 3, the DSF values of the 4-story steel MRF building are plotted with respect to the four discrete seismic intensities. While the steel MRF building remained elastic (i.e., 20% and 40% of the JR Takatori record), the corresponding DSF values were on the order of 0.15 or less. For a design-basis seismic event, the peak story drift ratios were on the order of 2% along the height of the building; the corresponding DSF values were on the order of 0.20 to 0.30. For larger drifts, DSF values attained 1.0. Figure 3 suggests that while the story-based EDPs of the building increase the corresponding DSF value tends from zero to one. The EDP-DSF relation is further explored in Section 2.3.2.

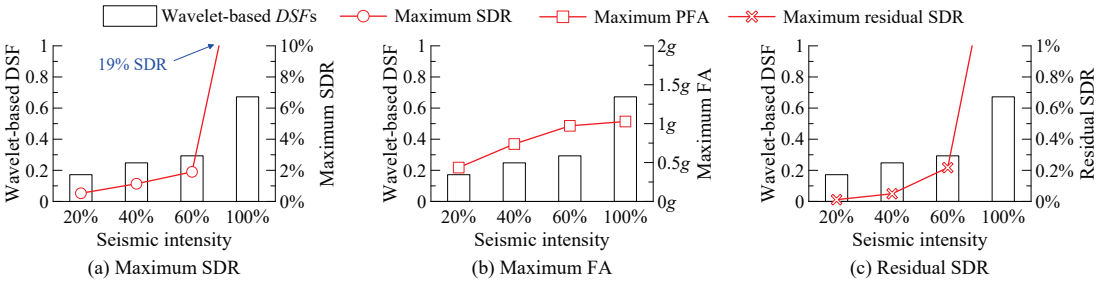

Figure 3: Wavelet-based DSF values in the y loading direction of the 4-story steel frame building with MRFs tested at E-Defense facility.

2.3. Approximate method for computing story-based EDPs

Figure 4 illustrates schematically how we developed the approximate method that maps the wavelet-based DSF with story-based EDPs at a given seismic intensity. Three phases of analysis are conducted: (i) nonlinear response history analyses (NRHAs) that employ nonlinear building models of representative steel MRF buildings to obtain simulated story-based EDPs and the roof absolute acceleration response histories of the respective building over a wide range of seismic intensities; (ii) wavelet analysis to obtain the wavelet-based DSFs (see Section 2); and (iii) stepwise multivariate linear regression analysis for the development of story-based EDP predictive models. The story-based EDPs of interest are the peak story drift ratio (SDR), residual SDRs and peak floor absolute accelerations (PFAs).

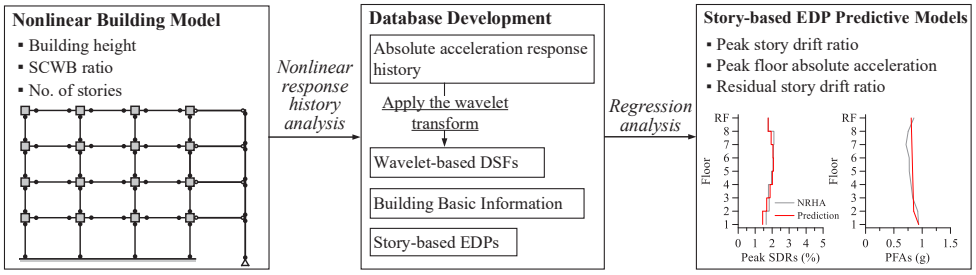

Figure 4: Flowchart for the development of the approximate method for story-based EDP computations.

2.3.1. Building response database development

In order to populate the best-suited damage indicators (i.e., wavelet-based DSFs) discussed later on in Section 3.2 a wide range of archetype steel frame buildings with MRFs is considered. In particular, the archetypes range from 1 to 20 stories. Their steel MRFs are designed with three strong-column/weak-beam (SCWB) ratios of 1.0 (i.e., code-based design), 1.5 and 2.0 in accordance with current seismic provisions in North America [30, 31]. Figure 5 illustrates a plan view and elevation of a representative 8-story steel frame building with perimeter MRFs. Detailed information about the design details of the archetypes can be found in [32–34].

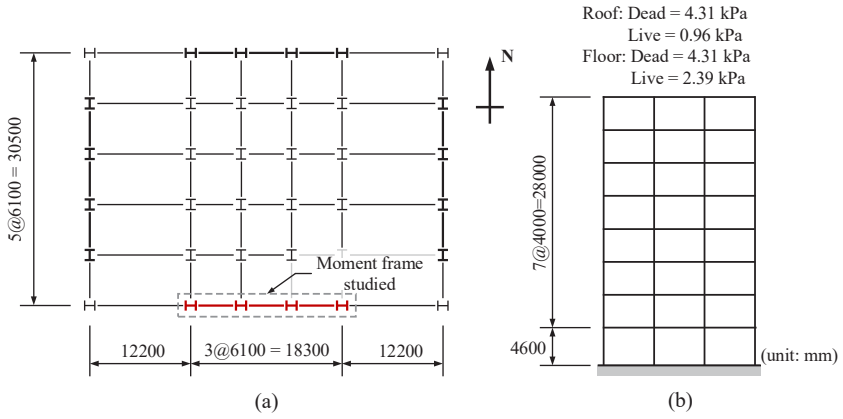

Figure 5: Typical 8-story archetype steel frame building: (a) plan view; and (b) elevation.

2.3.2. *Nonlinear building models*

Two-dimensional (2-D) nonlinear model representations of all the archetype MRFs in the east-west (E-W) loading direction are developed and implemented in the Open System for Earthquake Engineering Simulation (OPENSEES) Platform [35]. Referring to Figure 5(a), these MRFs are shown in the highlighted dashed box. The MRF steel beams and columns are modeled with elastic beam-column elements and lumped-plasticity flexural hinges at their ends as shown in Figure 6(a). The phenomenological model that was developed by Ibarra et al. [36] and refined and calibrated by [37, 38], is utilized to simulate cyclic and in-cycle strength and stiffness deterioration. Figure 6(b) illustrates a comparison between the simulated beam moment-chord rotation relations and the one deduced from a full-scale experiment conducted by Gilton et al. [39]. Referring to Figure 6(a), the nonlinear building model also considers explicitly the beam-to-column joint panel zone. The Krawinkler model [40] is employed for this purpose. Second order geometric effects are considered with a fictitious leaning column as shown in Figure 6(a). Damping is idealized with the Rayleigh model. Two percent damping ratio ($\zeta = 2\%$) is assigned to the first and third modes of all the nonlinear building models as discussed in Elkady and Lignos [33, 34].

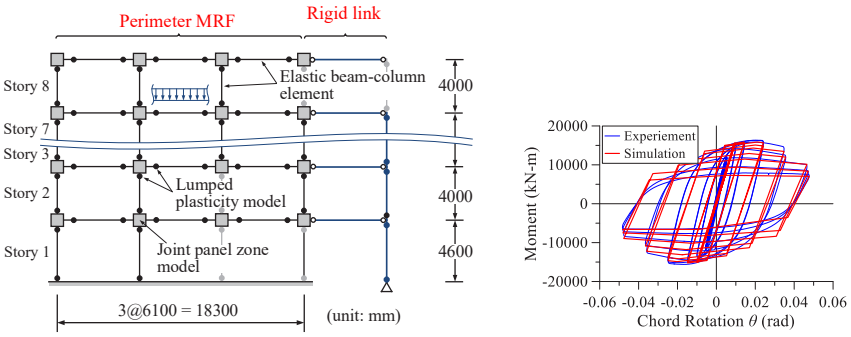

Figure 6: Example of nonlinear building model representation: (a) 2-D numerical model of the 8-story steel frame building; and (b) component deterioration model validation (data from Gilton et al. [39]).

Multiple NRHAs (i.e., incremental dynamic analysis, IDA) [41] are performed based on a suite of ground motions with large moment-magnitude, $6.5 \leq M_w \leq 7$ and short closest-to-fault-rupture distance, 13 km $< R_{rup} <$ 40 km that represents the seismic hazard at the design location [42]. The story-based EDPs (i.e., peak SDRs, residual SDRs, and PFAs) are obtained for each ground motion over a wide range of seismic intensities. The wavelet-based DSFs are determined from the absolute acceleration response histories recorded at the roof of each archetype building as discussed in Section 2.2. Figure 7 shows the wavelet-based DSFs with respect to the peak SDRs of the 8-story archetype at stories 1, 2 and 8. In steel MRFs large story drift demands are expected to saturate near the bottom stories at low probability of occurrence earthquakes [40]. Referring to Figure 7, this is depicted by the employed DSF. A more rapid slope of the peak SDR – DSF relation indicates that in this particular story the structural damage is very evident. Same observations hold true for the rest of the story-based EDPs of interest but are not shown herein due to brevity.

The database of nonlinear building responses as well as the mapped wavelet-based DSF values are employed to develop empirical equations that predict the story-based EDPs of interest given a seismic intensity.

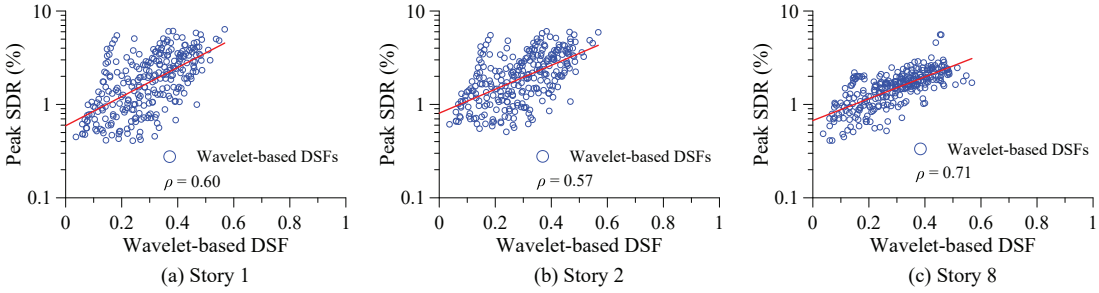

Figure 7: Scatter plots of wavelet-based DSF versus peak SDRs of the 8-story MRF building.

2.3.3. Proposed relationships for rapid earthquake-induced damage assessment

A stepwise multivariate linear regression analysis [43] is employed to establish *a priori* the relation between the building responses (i.e., story-based EDPs along the building height) and several predictor variables. These relationships are based on the building response database discussed in Section 2.3.2. The empirical equations consider only statistically significant predictor variables. Equation (10) represents the general functional form for estimating median story-based EDPs,

$$\ln(EDP_i) = \beta_0 + \beta_1 \cdot \ln(IM) + \beta_2 \cdot (DSF) + \beta_3 \cdot (h_x/H) + \beta_4 \cdot (h_x/H)^2 + \beta_5 \cdot (h_x/H)^3 + \beta_6 \cdot (SCWB) + \beta_7 \cdot (N) + \beta_8 \cdot (N)^2 + \varepsilon \tag{10}$$

in which β_i are the regression constants; ε is the random error (i.e., residual); EDP_i are the corresponding peak SDRs, residual SDRs and PFAs at level i. Referring to Eq. (10), it was found that the average spectral acceleration S_{avg}

Table 1: Range of predictor variables for peak story-based EDPs based on the building response database.

	S_{avg} (g)	PGA (g)	h_x/H	*SCWB*	N
Minimum	0.02	0.05	0.05	1.00	2.00
Maximum	1.61	7.17	1.00	2.00	20.00
Mean	0.25	1.17	0.56	1.53	11.31
Standard deviation	0.18	0.97	0.29	0.41	5.67
COV	0.03	0.94	0.08	0.16	32.16

proposed by [44–46] provides best estimates of peak and residual SDRs compared to other seismic intensity measures (IMs) (e.g., pseudo-acceleration (S_a), peak ground acceleration (*PGA*), peak ground velocity (*PGV*), Arias intensity (I_a) [47]) that were examined. The S_{avg} is computed as the geometric mean of 5% damped spectral accelerations ranging between $0.2T_1$ and $3T_1$ with a uniform interval of 0.01s [46, 48] based on the horizontal component of excitation in the loading direction of interest; T_1 is the first-mode period of the building under consideration. Similarly, the *PGA* was found to provide better estimates for PFAs compared to other IMs that were examined. Notably, the FEMA P-58 simplified approach [9] utilizes the same IM for computing PFAs along the building height. In order to compute the S_{avg} and *PGA* after an earthquake an acceleration sensor should be placed at the ground floor of the building. If the base motion is not available, the output-only system identification method proposed by Lignos and Miranda [49] may be used to obtain the input ground motion. Furthermore, a number of alternatives to simplify Eq. (10) to the extent possible without sacrificing the prediction accuracy were considered. In certain cases, the DSF was excluded from the regression model; however, the corresponding functional form lead to a 45% under-prediction of EDPs at seismic intensities associated with a Design Basis and a Maximum Considered Earthquake.

Referring to Eq. (10), the wavelet-based *DSF* is determined from the absolute acceleration response history recorded at the building roof; h_x is the height above the base of the building to floor level x; H is the total building height above the ground; *SCWB* is the strong-column/weak-beam ratio determined by the year of building construction and regional seismic provisions; and N is the number of stories of the building under consideration. Equation (10) includes the term h_x/H to reflect the variability of EDPs as a function of the story. Table 1 summarizes the range of applicability of Eq. (10). The same table provides the minimum, maximum, mean, standard deviation, and coefficient of variation (COV) of the building response database.

To treat the statistical error and associated uncertainty in the regression model, t- and F-statistics are performed at a 5% significance level. Tables 2 and 3 summarize the intercepts, the regression coefficients and their p-values in the t-statistic and the F-statistic, the coefficient of determination R^2 and standard deviation $\sigma_{\ln}$ for buildings with less than 8 stories and buildings with more than 9 stories, respectively. Referring to Tables 2 and 3, all the considered predictor variables significantly affect the accuracy of the models. In particular, the p-values in the t-statistic are zero.

Referring to Tables 2 and 3, the R^2 of the residual SDR is smaller than the corresponding values for the peak SDRs and PFAs. The residual SDR is influenced much more than other EDPs by the component modeling parameters and the record-to-record variability [8, 10, 50–53].

Table 2: Regression coefficients for story-based EDPs of steel frame buildings with less than 8 stories.

Predictor variables	Peak SDR			PFA			Residual SDR		
	Coefficient	t-statistic	p-value	Coefficient	t-statistic	p-value	Coefficient	t-statistic	p-value
$\ln\left(S_{avg}\right)$	0.69	140.55	0.00	–	–	–	0.57	61.80	0.00
$\ln(PGA)$	–	–	–	0.63	213.30	0.00	–	–	–
DSFs	0.34	11.54	0.00	0.12	5.64	0.00	0.55	3.59	0.00
h_x/H	-1.75	39.38	0.00	-0.06	-9.73	0.00	0.22	2.71	0.01
$(h_x/H)^2$	-1.34	-36.95	0.00	–	–	–	-0.32	-4.82	0.00
$(h_x/H)^3$	–	–	–	–	–	–	–	–	–
$SCWB$	-0.09	-14.09	0.00	0.08	18.99	0.00	-0.09	-8.01	0.00
N	0.42	36.24	0.00	-0.21	-28.92	0.00	0.42	18.57	0.00
N^2	-0.04	-36.60	0.00	0.02	26.39	0.00	-0.04	-18.52	0.00
	Intercept=-4.43, F=6.24$\times 10^3$, p-value=0, R^2=0.77, $\sigma_{\ln}$=0.29			Intercept=0.38, F=1.56$\times 10^4$, p-value=0, R^2=0.88, $\sigma_{\ln}$=0.20			Intercept=-5.22, F=1.04$\times 10^3$, p-value=0, R^2=0.39, $\sigma_{\ln}$=0.53		

Table 3: Regression coefficients for story-based EDPs of steel frame buildings with 9 to 20 stories.

Predictor variables	Peak SDR			PFA			Residual SDR		
	Coefficient	t-statistic	p-value	Coefficient	t-statistic	p-value	Coefficient	t-statistic	p-value
$\ln\left(S_{avg}\right)$	0.52	135.86	0.00	–	–	–	0.32	0.32	0.00
$\ln(PGA)$	–	–	–	0.61	270.96	0.00	–	–	–
DSFs	0.76	33.20	0.00	0.34	20.80	0.00	0.62	16.53	0.00
h_x/H	3.89	44.40	0.00	-0.96	-53.05	0.00	0.78	15.49	0.00
$(h_x/H)^2$	-7.16	-39.03	0.00	0.83	51.46	0.00	-0.99	-21.89	0.00
$(h_x/H)^3$	3.82	34.27	0.00	–	–	–	–	–	–
$SCWB$	-0.10	-19.77	0.00	0.03	9.68	0.00	-0.07	-8.08	0.00
N	0.11	25.85	0.00	-0.07	-27.82	0.00	0.14	20.32	0.00
N^2	-0.004	-25.11	0.00	0.002	23.44	0.00	-0.005	-19.81	0.00
	Intercept=-4.49, F=5.55$\times 10^3$, p-value=0, R^2=0.76, $\sigma_{\ln}$=0.32			Intercept=0.37, F=2.84$\times 10^4$, p-value=0, R^2=0.89, $\sigma_{\ln}$=0.19			Intercept=-5.51, F=1.11$\times 10^3$, p-value=0, R^2=0.23, $\sigma_{\ln}$=0.53		

Referring to Figure 8, indicative box whisker plots of the residuals against predictor variables are shown for steel frame buildings with less than 8 stories; the centerline and the bottom/top of the box represent the median and the 25th/75th percentiles of the residuals against predictor variables. The box whiskers show the 10th/90th percentile information of the grouped data. From this figure, the box whisker plots do not suggest any explicit dependency of the residuals on each predictor variable. In particular, the residuals fall within a horizontal band around zero. Furthermore, the normal probability plot (i.e., Q-Q plot [43]) shows that the residual points lie approximately on a straight line. A slight deviation from the straight line is only observed in the tails of the Q-Q plot. Therefore, the distribution of the residuals may be regarded as normal [43] with a zero mean and a standard deviation found from the residual analysis. Same observations hold true for steel frame buildings with 9 to 20 stories.

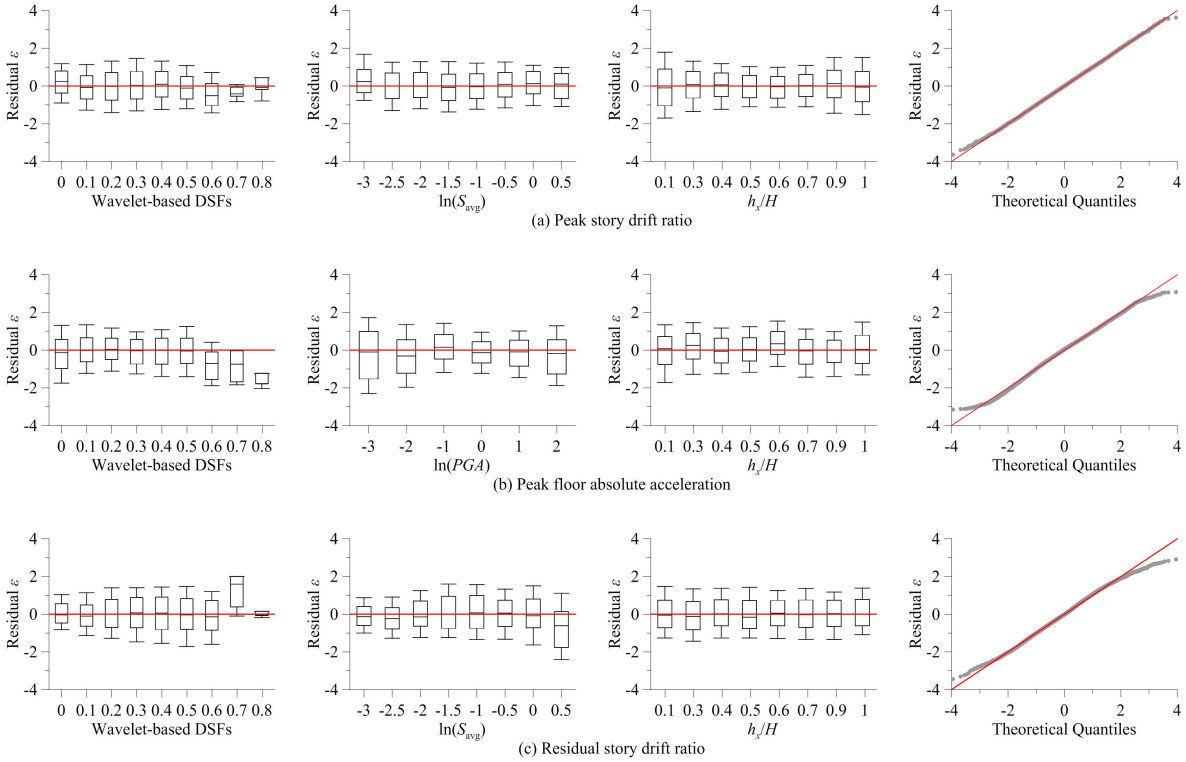

Figure 8: Diagnostic residual plots for story-based EDPs of steel frame buildings with 8 stories or less.

The efficiency of Eq. (10) in predicting story-based EDPs is further illustrated for selected seismic intensities that represent hazard levels of interest to the engineering profession: namely (i) a service-level earthquake (i.e., SLE: seismic hazard level of 50% probability of exceedance in 50 years); (ii) a design-basis earthquake (i.e., DBE: seismic hazard level of 10% probability of exceedance in 50 years); and (iii) a maximum considered earthquake (i.e., MCE: seismic hazard level of 2% probability of exceedance in 50 years). Figures 9 and 10 show the box-whisker plot of simulated-to-predicted EDP ratios (i.e., residuals) at the three seismic hazard levels of interest for an 8- and a 12-story steel frame building, respectively. Referring to Figures 9 and 10, the centerline and the box edges indicate the median

and the 25th/75th percentiles of the predicted story-based EDPs. The box whiskers extend to the 10th/90th percentiles of the simulated-to-predicted EDP ratio. From the same figures, Eq. (10) slightly overestimates the peak SDRs and PFAs in the lower stories of both buildings at the SLE seismic intensity (i.e., approximately 30% to the maximum relative to NRHA results). It is evident that the predictive equations provide reasonable estimates of peak SDRs and PFAs along the height of the steel frame buildings at the DBE and MCE seismic intensities.

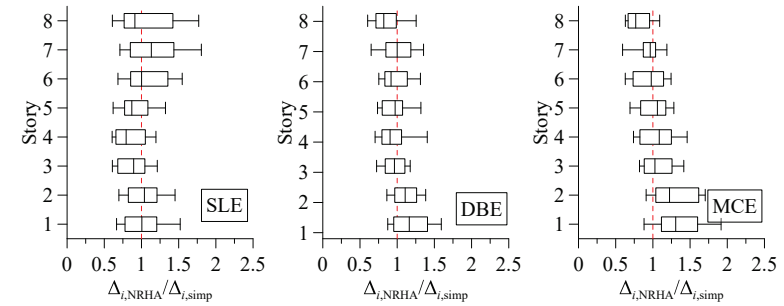

(a) Peak story drift ratios

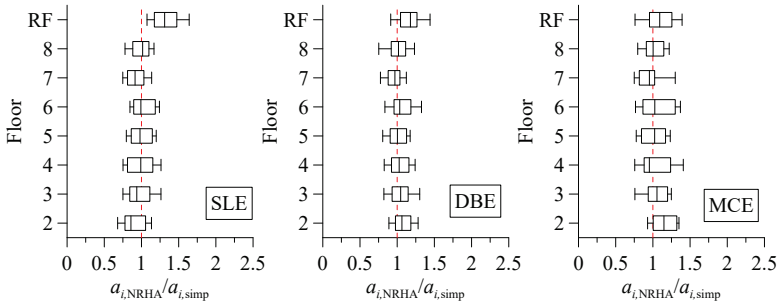

(b) Peak floor absolute accelerations

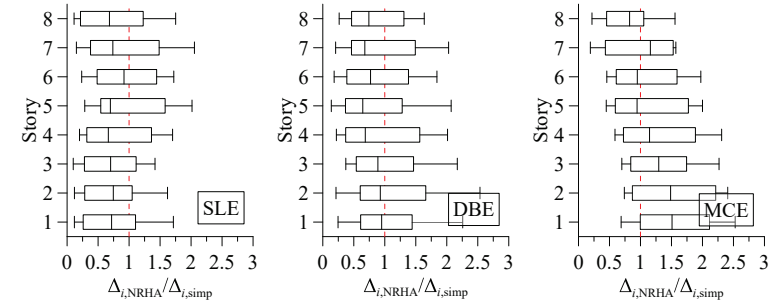

(c) Residual story drift ratios

Figure 9: Diagnostic residual plots for the 8-story steel frame building designed with SCWB $\geq$ 1.0.

Referring to Figures 9(c) and 10(c), Eq. (10) generally tends to overestimate the median residual SDRs (i.e., $\Delta_{i,NRHA}/\Delta_{i,simp} \leq 1.0$). This is mainly attributed to the influence of the record-to-record variability and input model parameters on the residual drift demands along the height of a building [10, 54]. The median values of simulated-to-predicted residual SDR ratio for steel frame buildings of interest are between 0.5 and 1.75. Same observations hold

true for the rest of the cases included in the building response database discussed in Section 2.3.2.

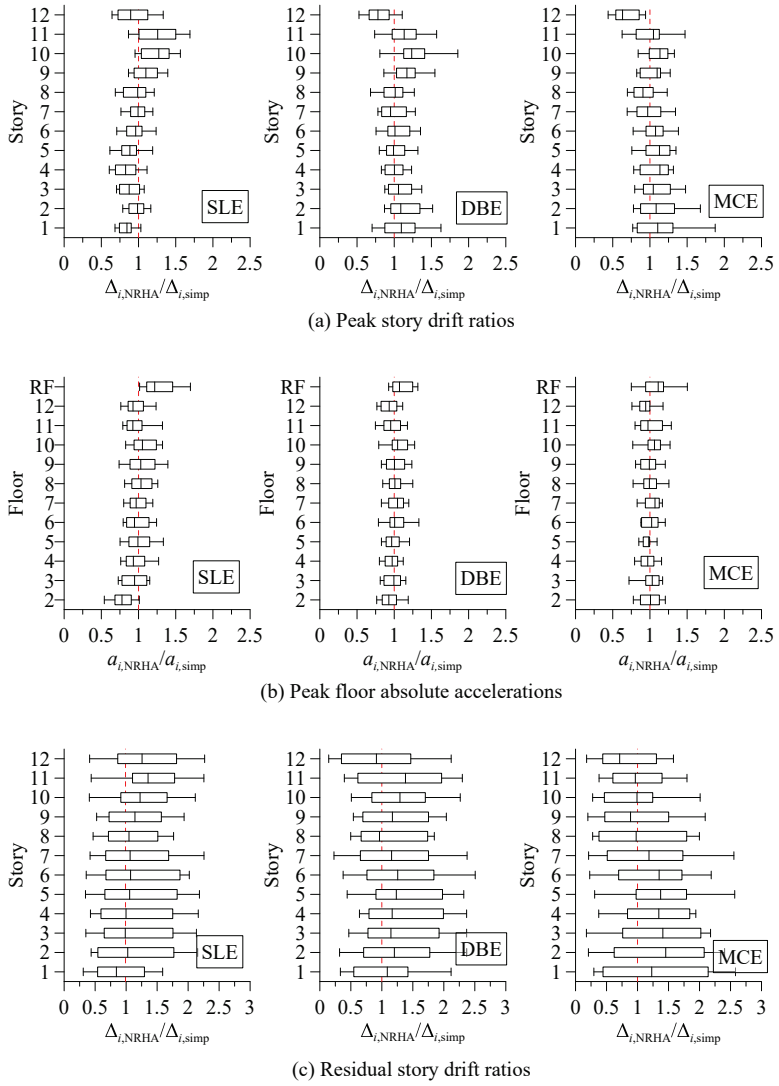

(a) Peak story drift ratios

(b) Peak floor absolute accelerations

(c) Residual story drift ratios

Figure 10: Diagnostic residual plots for the 12-story steel frame building designed with SCWB $\geq$ 1.0.

2.3.4. Comparisons of proposed nonmodel-based method with available predictive models

In this section, the efficiency of the proposed nonmodel-based method in predicting story-based EDPs in steel frame buildings with MRFs is evaluated with regards to results obtained from rigorous NRHA. For this purpose, the 8-story steel frame building utilized in Section 2.3.3 is employed. This building is subjected to the far-field set of 44 ground motions retrieved from FEMA P695 [55]. For comparison purposes the FEMA P-58 simplified procedure [9] is also considered. This procedure requires an explicit building model for the story-based EDP computations. This model should appropriately represent the distribution of mass and stiffness along the height of the building. On the basis of the FEMA P-58 simplified approach [9] we utilized (i) linear and nonlinear building models; (ii) an elastic

234 analysis based on a first-mode lateral force distribution; and (iii) an estimate of the building's lateral yield strength.
235 This was computed through nonlinear static analysis based on a first-mode lateral load pattern.

236 Figure 11 depicts the predicted peak SDRs along the height of the 8-story steel frame building based on the
237 proposed method in comparison with the median peak SDR demands from NRHA for three seismic hazard levels
238 (i.e., SLE, DBE and MCE) as defined at the design location of interest. In the same figure, we have superimposed the
239 predicted median peak SDRs based on the FEMA P-58 simplified procedure [9]. To facilitate a lower/upper bound
240 analysis, the 16th/84th percentiles of peak SDRs, PFAs and residual SDRs are provided in the same figures.

241 Referring to Figure 11(a), it is evident that the proposed predictive equations provide reasonable estimates of peak
242 SDRs regardless of the seismic intensity. Notably, the only input information that is required is the building height,
243 the employed SCWB ratio and the computed wavelet-based DSF based on the absolute acceleration response history
244 at the roof of the 8-story building. Figure 11(a) suggests that the proposed method provides better estimates of median
245 peak SDR demands compared to those obtained from the FEMA P-58 simplified procedure regardless of the seismic
246 intensity of interest. In particular, at the MCE seismic intensity, the differences of the predicted peak SDRs relative
247 to those determined by NRHA are on average, 12% and 23% based the proposed nonmodel method and the FEMA
248 P-58 simplified procedure, respectively. Referring to Figure 11(a), the FEMA P-58 simplified procedure significantly
249 overestimates the peak SDRs in the upper stories of the 8-story building at the MCE intensity. This approach is not
250 applicable when peak SDRs exceed four times the corresponding yield drift ratio and/or excessive deterioration in
251 strength and stiffness of structural components occurs [9]. On the other hand, the proposed nonmodel-based approach
252 predicts well the peak SDR demands over the building height for the same seismic intensity.

253 Referring to Figure 11(b), the predicted median PFAs along the height of the 8-story steel frame building are
254 shown for the three selected levels of seismic intensity. Superimposed in the same figure is the median PFA demands
255 from NRHA. From this figure, it is found that the proposed method provides reasonable PFA estimates along the
256 height of the building for moderate to severe seismic intensities (i.e., DBE and MCE). At frequently occurring seismic
257 intensities (i.e., SLE), the proposed approach seems to underestimate PFAs by approximate 16%, on average, relative
258 to NRHA results. Similar accuracy is achieved with the FEMA P-58 simplified approach.

259 Similarly, Figure 11(c) compares the predicted residual SDRs along the height of the 8-story steel frame building
260 based on the proposed approach and the FEMA P-58 simplified approach for the three seismic intensities. In the
261 same figure, we have superimposed the median response based on NRHA. Referring to Figure 11(c), the proposed
262 approach tends to slightly overestimate the residual SDRs at the mid-height of the building whereas the FEMA P-58
263 simplified approach tends to underestimate the residual SDRs at the bottom stories of the building. This is not the
264 case at higher seismic intensities associated with low probability of occurrence earthquakes (i.e., MCE). Previous
265 research has identified that residual drifts are highly variable and very sensitive to the earthquake magnitude, distance
266 to the source range, the adopted component hysteretic behavior as well as the analytical model representations of a
267 building [10, 52, 56, 57]. For the aforementioned reasons, it is recommended that a lower/upper bound analysis should
268 be employed based on the 16th/84th percentile of the predicted values of the proposed approach as shown in Figure

11(c). In this case, the median response from NRHA is within these two percentiles. Same observations hold true for buildings with 9 to 20 stories but are not shown here due to brevity.

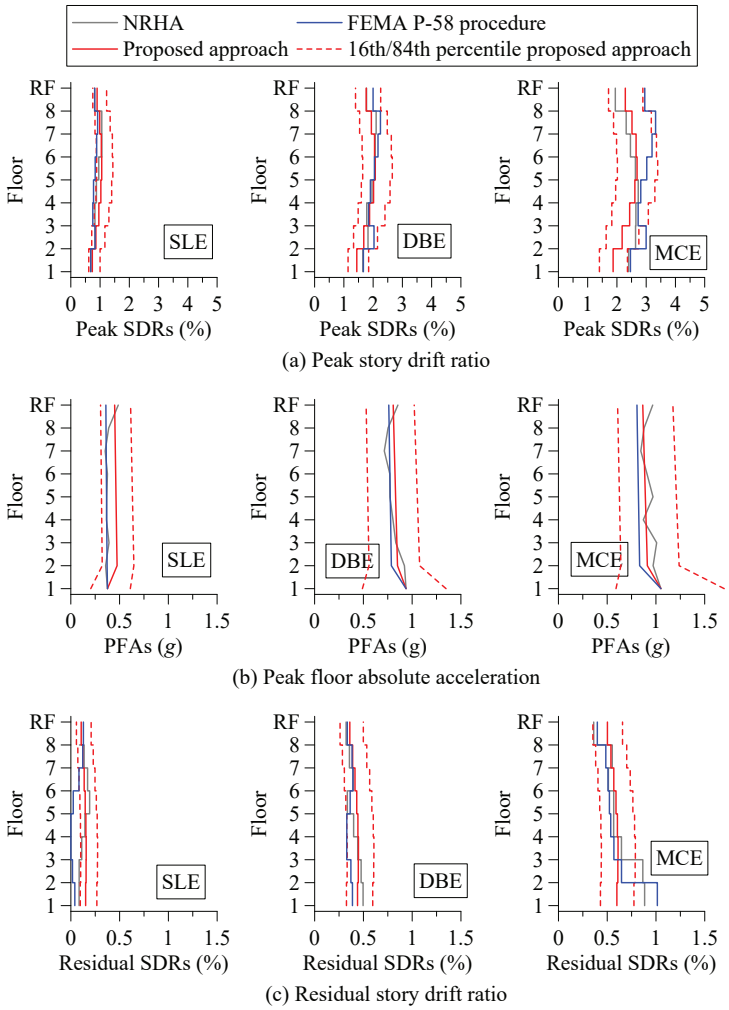

Figure 11: Predicted versus simulated story-based EDPs along the height of the 8-story steel frame building designed with SCWB $\geq$ 1.0.

3. Application of simplified seismic assessment methodology in instrumented steel frame buildings

3.1. Case study instrumented building

The proposed approach could be employed for the rapid seismic assessment of instrumented steel frame buildings with fairly low instrumentation density. In particular, two sensors at each principal axis are only required along the height of the respective building. Preferably, one sensor should be placed at the base to obtain the peak ground acceleration; and the second one should be placed at the building roof to obtain the wavelet-based DSF. If sensors in other locations of the building are available then the output-only system identification technique proposed by Lignos and Miranda [49] could be employed to obtain the absolute acceleration histories at the base and roof of the building

of interest. In that respect, the proposed approach may significantly reduce the cost of installation, operation, and computation of a large volume of sensors and data.

The proposed approach is evaluated with the use of recorded data from an instrumented 15-story steel frame building that was located in Los Angeles, California (34.058°N, 118.250°W) and experienced the 1994 Northridge earthquake. Its lateral load resisting system consists of steel MRFs. The building was designed in 1961. Therefore, capacity design principles were not formally employed. However, the design of similar buildings was mostly governed by lateral wind loads over seismic loads, and the member properties were determined based on wind demands; therefore, they were detailed to behave in a ductile manner [58]. Considering the large column sizes that were typically employed to satisfy the axial and lateral drift limits in tall buildings, the column flexural strength was not deemed to be critical [58]. Therefore, the building had a SCWB ratio close to 1.0. The existence of the concrete shear walls up to the first story of the steel frame building did not seem to influence the seismic behavior of the steel frame building; in that sense, the lateral load resistance is primarily provided by the steel MRFs. Fifteen accelerometers were installed at four levels along the height of the building. The recorded data was retrieved from the Center for Engineering Strong Motion Data (CESMD) operated by the California Department of Conservation's Strong Motion Instrumentation Program (CSMIP) in cooperation with the US Geological Survey (USGS). The building station number was CSMIP 24569. The plan view and elevation of the building is shown in Figure 12.

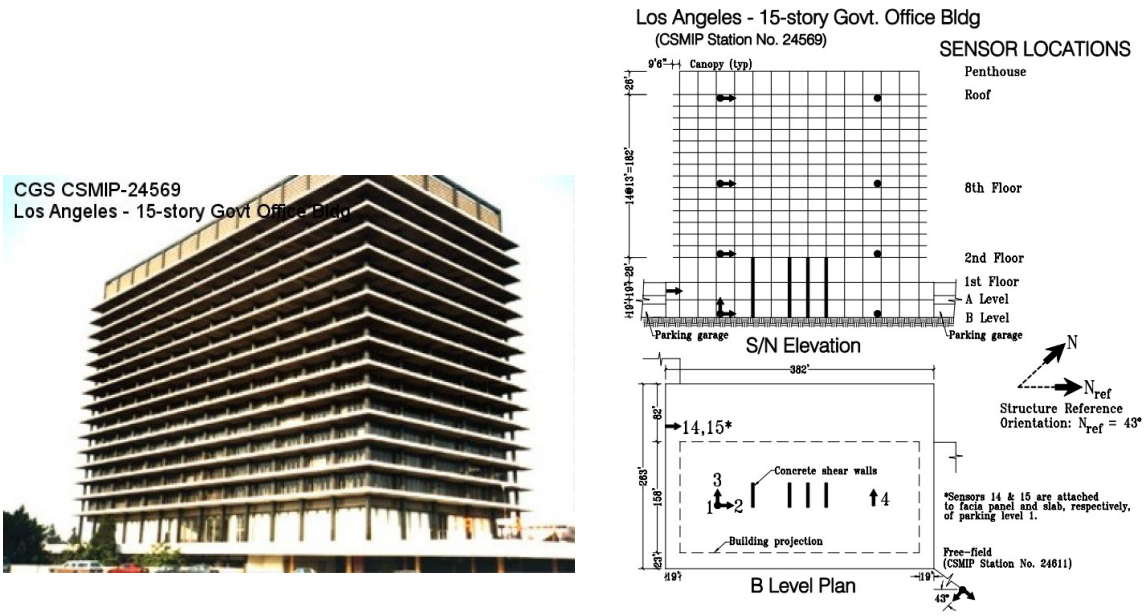

(a) (b)

Figure 12: Fifteen-story Government steel frame office building (CSMIP 24569); (a) overview; and (b) plan, and elevation view of the building (images from the US National Center for Engineering Strong Motion Data at http://strongmotioncenter.org).

3.2. *Predicted engineering demand parameters and earthquake-induced economic losses*

To determine the wavelet-based DSFs to be used in Eq. (10), the first-mode frequency f_1 of the building is identified in its two orthogonal loading directions based on the input base motion and the output absolute acceleration response histories recorded at the building roof during the earthquake based on the ARX method [14] (see Section 2.1). Table 4 summarizes the identified natural frequencies of the first two building modes in the two horizontal loading directions. The equivalent damping ratios, ζ_{eq} for the two modes per loading direction are also identified. The wavelet-based DSF is then determined from the recorded absolute acceleration response history at the building roof.

Table 4: System identification for the 15-story instrumented steel frame office building in Los Angeles.

Loading direction	Mode	Natural frequency f (Hz)	Equivalent damping ratio, ζ_{eq} (%)
North-South	1st	0.34	2.2
	2nd	0.92	3.8
East-West	1st	0.32	3.4
	2nd	0.90	2.3

Figure 13 shows the estimated story-based EDPs of the 15-story building for both loading directions [i.e., North-South (NS) and East-West (EW) directions]. These EDPs are computed within few seconds based on Eq. (10) and the corresponding values from Table 3. Referring to Figure 13(c), the recorded PFAs at three floor levels are superimposed for comparison purposes. It is found that the proposed nonmodel-based approach provides accurate estimates of the building's PFAs. Referring to Figures 13(a) and 13(b), the proposed approach predicts that the peak SDR and residual SDR along the height of the same building is 1.30% and 0.35%, respectively. This occurred around the mid-height of the building in both loading directions of interest. Therefore, the building experienced fairly minor structural damage due to flexural steel beam yielding. Notably, the FEMA P-58 simplified approach cannot be directly utilized for the seismic performance assessment of the same building because the building geometry as well as the material properties of the respective structural components should be known upfront. Furthermore, a considerable time investment is needed for the nonlinear building model development and validation.

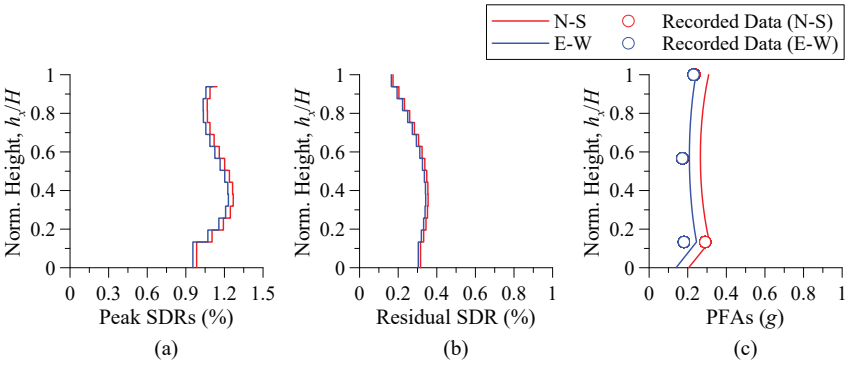

Figure 13: Predicted story-based EDPs for the 15-story Government steel frame office building (CSMIP 24569).

The predicted story-based EDPs can be further utilized to conduct a probabilistic building-specific economic loss assessment. The story-based building-specific loss estimation methodology proposed by Ramirez and Miranda [59] can be employed for this purpose. The three possible consequences of a building in the aftermath of an earthquake are considered as follows: (i) collapse does not occur and structural and/or non-structural components shall be repaired or replaced after the earthquake; (ii) collapse does not occur, but the building may be demolished and rebuilt due to excessive residual deformations; and (iii) collapse occurs and the building shall be rebuilt. Assuming that these consequences are mutually exclusive, the expected building losses conditioned on the seismic intensity *IM* are defined as follows,

$$\begin{aligned} E\left[L_T|IM\right] =& E\left[L_T|NC\cap R,IM\right]\cdot P\left(NC\cap R|IM\right)+E\left[L_T|NC\cap D,IM\right]\cdot P\left(NC\cap D|IM\right) \\ &+E\left[L_T|C,IM\right]\cdot P\left(C|IM\right) \end{aligned} \tag{11}$$

in which $E\left[L_T|NC\cap R,IM\right]$ is the expected total repair cost given that collapse does not occur and the building may be repaired at a given seismic intensity *IM= im*; $E\left[L_T|NC\cap D,IM\right]$ is the expected building loss when there is no collapse but the building may be demolished at a given seismic intensity *IM=im*; $E\left[L_T|C,IM\right]$ is the total replacement cost of the building when collapse occurs at a given seismic intensity *IM = im*, because the building needs to be replaced in this case. Furthermore, $P\left(NC\cap R|IM\right)$ is the probability that the building will not collapse but may be repaired or replaced conditioned on the seismic intensity *IM=im*; $P\left(NC\cap D|IM\right)$ is the probability that the building will not collapse but it may be demolished because of potentially large residual deformations conditioned on the seismic intensity *IM=im*; $P\left(C|IM\right)$ is the probability of collapse conditioned on the seismic intensity *IM=im*. The expected total repair cost conditioned on the building not collapsing $E\left[L_T|NC\cap R,IM\right]$ is defined as follows,

$$E\left[L_T|NC\cap R,IM\right]=\sum_{i=1}^{m}\sum_{j=0}^{n}\int_0^{\infty}E\left[L_{ij}\left|DS_{ij}\right.\right]P_{DS_{ij}|EDP}\,f_{EDP|IM}\,\mathrm{d}EDP \tag{12}$$

in which *m* is the number of damageable components being considered; *n* is the number of damage states a component may experience; $E\left[L_{ij}|DS_{ij}\right]$ is the mean repair cost for the *i*th component being in the *j*th damage state; $P_{DS_{ij}|EDP}$ is the probability of the EDP of interest associated with the *i*th component being in the *j*th damage state given an *EDP=edp*. The probability of having to demolish the building conditioned on the seismic intensity $P\left(NC\cap D|IM\right)$ is modeled by a lognormal distribution with a median $\mu_{D|RSDR}$ of 0.015 radians and a logarithmic standards deviation $\beta_{\ln D|RSDR}$ of 0.3 as proposed in [59]. More details about the mathematical formulation of the building-specific loss estimation methodology can be found in [59].

In order to reliably quantify the earthquake-induced losses of the instrumented building, the authors adopted a library of fragility curves of building components from FEMA P-58 [9]. Some of these curves were further refined by [54, 57]. The employed component fragility curves for the list of damageable components of the instrumented steel frame building are all listed in Table 5. Note that the suspended ceiling system in the instrumented building was assumed to be a typical US style with acoustic tiles, that is composed with both vertical and lateral supports,

grid members, boundary wall molding, and diagonal brace wires [60, 61]. The fragility curves for the elevator were assumed to be those of hydraulic elevators that were mostly installed in California in 1976 or later.

Although the building plan view was known (see Figure 12), its detailed architectural layout was not possible to be retrieved. The authors approximated the densities of various non-structural components and building content as discussed in Bradley et al. [65] in which the quantity of each non-structural component per square meter is determined according to the Mitrani-Reiser [66] methodology.

The fragility curves developed by Ramirez et al. [62] were adopted for pre-Northridge beam-to-column moment connections. An example of such curves is shown in Figure 14(a) for steel beams in pre-Northridge beam-to-column connections made of A36 steel. Referring to Figure 13(a), the probability of beam yielding at a peak SDR of 1.30% is more than 70%. The probability of premature fracture is slightly above 20% for the same peak SDR. For comparison purposes, the fragility curves of typical post-Northridge fully-restrained beam-to-column connections [67] are also shown in Figure 14(a). In this case, the likelihood of ductile fracture due to low-cycle fatigue is practically zero.

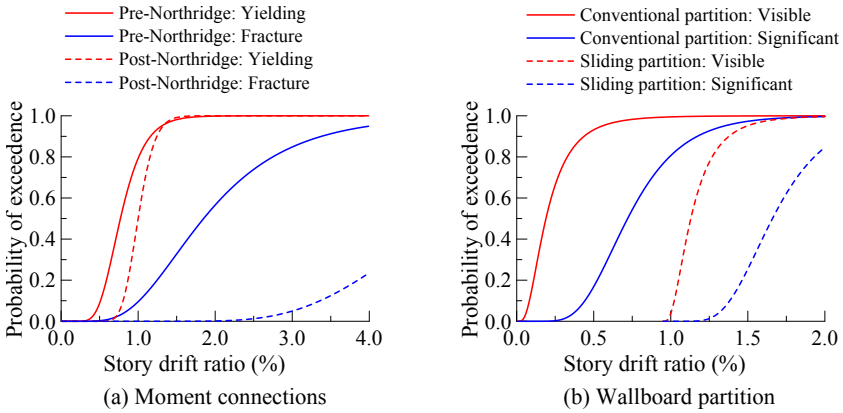

Figure 14: Fragility curves for typical pre- and post-Northridge fully-restrained beam-to-column connections and conventional and sliding gypsum wallboard partitions.

Figure 14(b) illustrates the fragility curves of conventional gypsum wallboard partitions [63] employed in this paper. The fragility curves of improved partitions [63] (i.e., sliding wallboard partitions that accommodate the expected SDR demand) are also shown in the same figure for comparison purposes. Referring to Figure 14(b), at a given SDR of 0.5%, the probability that the conventional wallboard partitions are in the minor damage state (i.e., visible) is over 70%. In this case the wallboard partitions can be repaired by means of patching, re-taping, sanding and painting the gypsum wallboard [63]. On the other hand, the probability of having visible damage in the improved partitions is zero for the same SDR. Table 5 also summarizes the repair cost per damage state for each building component including the respective fragility curve obtained from prior studies [9, 56, 62–64].

Figure 15 shows the expected earthquake-induced losses of the 15-story Government steel frame office building. The expected losses are normalized with respect to the total replacement cost of the building. Note that the total

Table 5: Fragility and cost estimates for the 15-story Government steel frame office building.

Assembly description	Damage state	Unit	Fragility parameters			Repair cost
			EDP	x_m	β	x_m ($)
Columns base (W $<$ 223kg/m) ([9])	Crack initiation	EA	SDR	0.04	0.40	19,224
	Crack propagation			0.07	0.40	27,263
	Fracture			0.10	0.40	32,423
Columns base (223kg/m $<$ W $\leq$ 446kg/m) ([9])	Crack initiation	EA	SDR	0.04	0.40	20,082
	Crack propagation			0.07	0.40	29,395
	Fracture			0.10	0.40	36,657
Columns base (W $>$ 446kg/m) ([9])	Crack initiation	EA	SDR	0.04	0.40	21,363
	Crack propagation			0.07	0.40	32,567
	Fracture			0.10	0.40	41,890
Column splices (W $<$ 223kg/m) ([9])	Crack initiation	EA	SDR	0.04	0.40	9446
	Crack propagation			0.07	0.40	11,246
	Fracture			0.10	0.40	38,473
Column splices (223kg/m $<$ W $\leq$ 446kg/m) ([9])	Crack initiation	EA	SDR	0.04	0.40	10,246
	Crack propagation			0.07	0.40	13,012
	Fracture			0.10	0.40	42,533
Column splices (W $>$ 446kg/m) ([9])	Crack initiation	EA	SDR	0.04	0.40	11446
	Crack propagation			0.07	0.40	14,812
	Fracture			0.10	0.40	47,594
Column ($\leq$ W27) ([9])	LB	EA	SDR	0.03	0.30	16,033
	LTB			0.04	0.30	25,933
	Fracture			0.05	0.30	25,933
Column ($\geq$ W30) ([9])	LB	EA	SDR	0.03	0.30	17,033
	LTB			0.04	0.30	28,433
	Fracture			0.05	0.30	28,433
Pre-Northridge moment connection (A36 steel, one-sided, $\leq$ W27) ([62])	Yielding	EA	SDR	0.0077	0.32	0
	Fracture	EA		0.0185	0.47	11,980
Pre-Northridge moment connection (A36 steel, one-sided, $\geq$ W30) ([62])	Yielding	EA	SDR	0.0077	0.32	0
	Fracture	EA		0.0185	0.47	12,313
Pre-Northridge moment connection (A36 steel, two-sided, $\leq$ W27) ([62])	Yielding	EA	SDR	0.0077	0.32	0
	Fracture	EA		0.0185	0.47	16,653
Pre-Northridge moment connection (A36 steel, two-sided, $\geq$ W30) ([62])	Yielding	EA		0.0077	0.32	0
	Fracture	EA	SDR	0.0185	0.47	16,653
Shear tab connections ([9])	Yielding	EA	SDR	0.04	0.40	12,107
	Partial tearing			0.08	0.40	12,357
	Complete separation			0.11	0.40	12,307
Corrugated slab (90mm steel; 100mm overlay) ([56])	Crack initiations	m^2	SDR	0.00375	0.13	180
	Crushing near column			0.01	0.22	330
	Shear stud fracture			0.05	0.35	570

Table 5: Fragility and cost estimates for the 15-story Government steel frame office building (continued).

Assembly description	Damage state	Unit	Fragility parameters			Repair cost
			EDP	x_m	β	x_m ($)
Wallboard partition ([63])	Visible	6m^2	SDR	0.0019	0.65	90
	Significant			0.0072	0.38	530
Wallboard partition finish ([63])	Visible	6m^2	SDR	0.0019	0.65	90
	Significant			0.0072	0.38	250
Exterior glazing ([64])	Crack	pane	SDR	0.04	0.36	440
	Fallout			0.046	0.33	440
Suspended ceiling ($A > 232$m^2) ([9])	5% tiles dislodge	232m^2	PFA (g)	0.35	0.40	3542
	30% tiles dislodge			0.55	0.40	29,337
	Collapse			0.80	0.40	55,200
Automatic sprinklers ([64])	Fracture	3.66m	PFA (g)	0.32	1.40	900
Elevator ([9])	Failure	EA	PGA (g)	0.50	0.28	3180

EDP, engineering demand parameter; LB, local buckling; LTB, lateral-torsional buckling; SDR, story drift ratio (unitless); PFA, peak floor absolute acceleration (g); PGA, peak ground acceleration (g); x_m, median value; β, lognormal standard deviation.

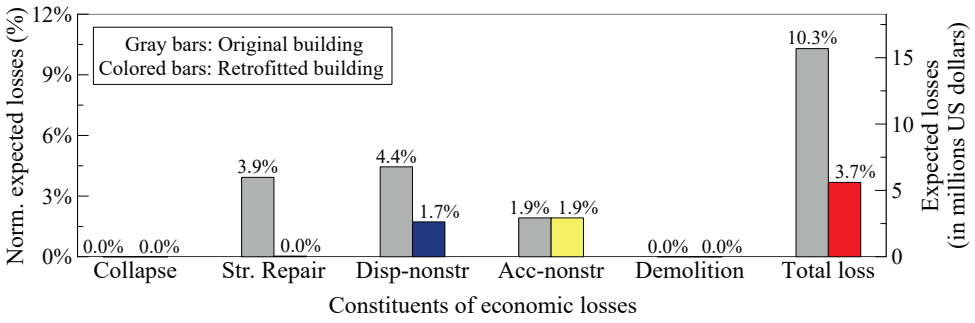

Figure 15: Normalized expected losses for 15-story Government steel frame office building (CSMIP 24569).

replacement cost of the building is determined for a given calendar year (i.e., 1994). Referring to Figure 15, the expected losses due to repairs slightly exceed 10% of the total replacement cost of the building. These losses are further disaggregated into structural/non-structural component repairs, building demolition, and collapse. For the given seismic intensity at the site of interest, losses due to collapse and demolition become negligible. This is to be expected given the amplitude of peak and residual SDRs along the height of the building [see Figure 13(a)]. However, drift-sensitive non-structural component repairs seem to be the major contributor to the expected building losses. On the other hand, the expected losses due to acceleration-sensitive non-structural component repairs are approximately 2.0% of the total replacement cost of the building. This seems to be a reasonable estimate based on the recorded maximum PFAs (i.e., 0.29g) along the height of the building. These PFA demands are much lower than the minimum seismic force limit (i.e., 0.5g) on acceleration-sensitive non-structural components at the design site [31].

Referring to Figure 15, the estimated losses due to structural damage are on the order of 4.4% of the total re-

placement cost of the building. Although the peak SDRs along the height of the building did not exceed 1.3% in both loading directions, repairs due to structural damage are primarily driven by the increased likelihood of premature fracture of pre-Northridge beam-to-column connections [62, 68]. To better "digest" these numbers, Figure 15 shows the normalized expected losses of the same building if it were to be built today with fully-restrained beam-to-column connections that utilize beams with reduced beam section (RBS) [67] and gypsum wallboard partitions that allow for sliding [63]. In this case, it is evident that the expected economic losses of the instrumented steel building would be reduced by a factor of 3, if it would be retrofitted with RBS connections and improved gypsum wallboard partitions.

3.3. Rapid Seismic Assessment at a "City-scale"

The proposed framework discussed in Section 2 offers the opportunity to conduct a rapid seismic risk and loss assessment of instrumented buildings at a "city-scale" for a given earthquake scenario. This concept is explored further by utilizing recorded data from an array of instrumented steel frame buildings with MRFs that experienced the 1994 Northridge earthquake. The recorded data were available through the CSMIP stations for the city of Los Angeles. Although the data is fairly scarce due to the density of the instrumented buildings at that time, the intention of the authors at this stage is to illustrate the concept of the generalized damage and expected loss maps at the city level. The accuracy of these maps can be further refined by either populating the number of instrumented buildings and/or by combining the proposed framework with other currently available tools that facilitate the city-scale rapid seismic assessment [16, 69–72].

Figures 16(a)–(c) show a generalized damage map for Los Angeles based on the maximum story-based EDP estimates that were computed along the height of the instrumented steel frame buildings that experienced the 1994 Northridge earthquake. The maps are developed with the use of ArcGIS (release version 10.3) [73]. In regions that instrumented data were not available, the contour maps were developed with a multivariate (spatial) interpolation. It was found that the inverse distance weighting (IDW) method [74] provides rational results in this case. This method assigns maximum values of EDPs to unknown points with a weighted average of the values available at the known points in the map. The mathematical form of the IDW method [74] is defined as follows,

$$z_{x,y} = \frac{\sum_{i=1}^{n} z_i w_i}{\sum_{i=1}^{n} w_i} \tag{13}$$

in which $z_{x,y}$ is the value to be estimated at the location point (x,y); and z_i represents the control value for the ith sample point. The weight w_i determines the relative importance of the individual control point z_i in the interpolation process as follows,

$$w_i = d_{x,y,i}^{-\beta} \tag{14}$$

in which $d_{x,y,i}$ is the distance between $z_{x,y}$ and z_i; and β is a user-defined exponent. In this study, the exponent β was assumed to be 2.0 as suggested in [73]. Equation (13) can be rewritten as follows,

$$z_{x,y} = \frac{\sum_{i=1}^{n} z_i d_{x,y,i}^{-\beta}}{\sum_{i=1}^{n} d_{x,y,i}^{-\beta}} \tag{15}$$

Referring to Figures 16(a)–(c), the area around the epicenter suffered the most structural and non-structural damage given the distribution of peak SDRs [see Figure 16(a)] and PFAs [see Figure 16(b)]. Notably, near the epicenter the peak SDRs and peak PFAs were on the order of 1.5% and $0.8g$, respectively. From the same figure, in the South-East of the city the distribution of the peak SDRs and PFAs were on the order of 0.5% and $0.4g$, respectively, indicating that the expected structural and non-structural damage would be fairly minimal in the same region. Referring to Figure 16(c), the distribution of residual SDRs was 0.45% or less; therefore, building demolition would not be a critical concern throughout Los Angeles. It is understood that the maps shown in Figures 16(a)–(c) can provide a first estimate of the post-earthquake safety of a city. These maps can be produced within minutes after the earthquake. In that sense, the proposed framework can be employed for city-scale management in the aftermath of an earthquake.

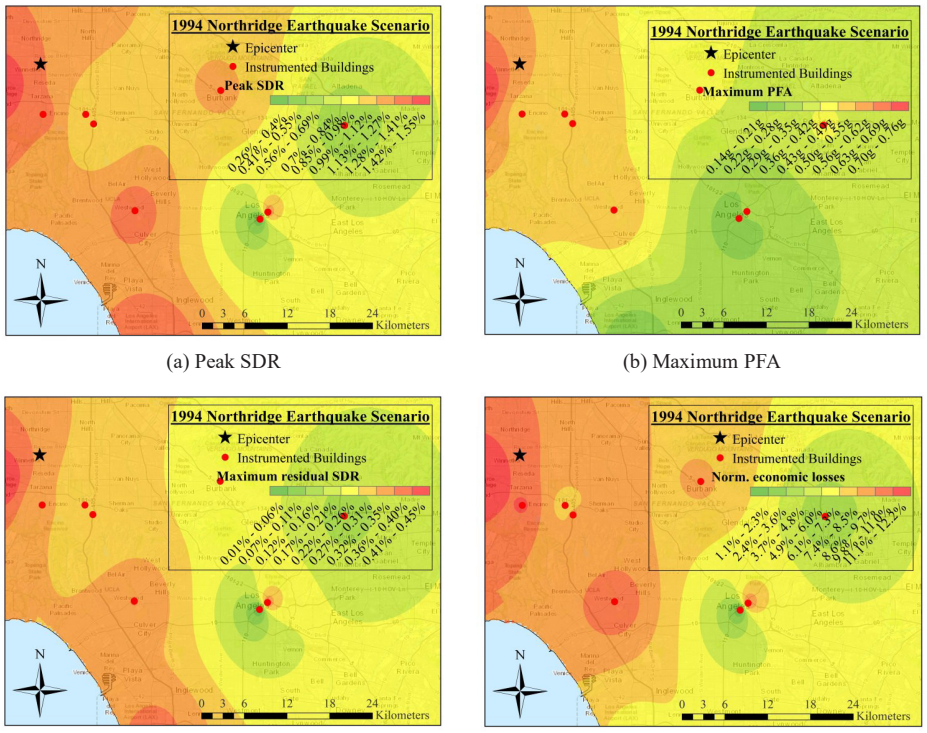

(a) Peak SDR

(b) Maximum PFA

(c) Maximum residual SDR

(d) Monetary loss distribution

Figure 16: "City-scale" generalized damage and expected loss maps for Los Angeles after the 1994 Northridge earthquake.

The computed story-based EDPs shown in Figures 16(a)–(c) can be further utilized to develop a generalized expected loss map for the same region. This map is shown in Figure 16(d). In this figure, the expected losses due to building repairs were computed as discussed in Section 3.2 and they were normalized with respect to the total

replacement cost of the respective building. Referring to Figure 16(d), steel frame buildings with MRFs located near the epicenter experienced monetary losses on the order of 12% of their total replacement cost due to damage in drift- and acceleration-sensitive non-structural components. From the same figure, the expected losses are dominated by repairs due to premature fracture in pre-Northridge beam-to-column connections. Referring to Figure 16(d), such failures were fairly minimal in the South-East of the city considering the magnitude of the peak SDRs and PFAs in this region. The expected losses for the city of Los Angeles after the earthquake are further disaggregated in Figure 17. In particular, Figures 17(a) and 17(b) illustrate the repairs needed due to premature fracture of pre-Northridge beam-to-column connections and damage in conventional gypsum wallboard partitions.

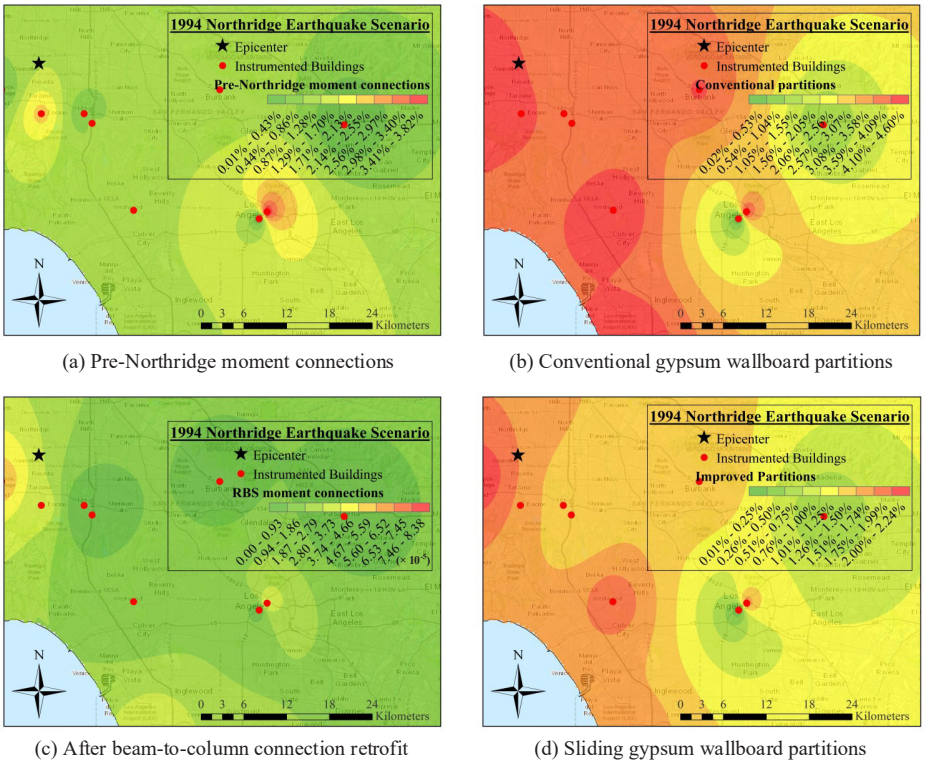

(a) Pre-Northridge moment connections

(b) Conventional gypsum wallboard partitions

(c) After beam-to-column connection retrofit

(d) Sliding gypsum wallboard partitions

Figure 17: Loss disaggregation maps for the city of Los Angeles after the 1994 Northridge earthquake; (a) losses due to repairs in pre-Northridge beam-to-column moment connections; (b) losses due to repairs in conventional gypsum wallboard partitions; (c) losses due to repairs in retrofitted beam-to-column moment connections; and (d) losses due to repairs in sliding gypsum wallboard partitions.

The generalized loss maps shown herein can be easily employed for the computation of the expected losses at a city-scale for a given earthquake scenario such that proper pre-disaster measures can be prioritized by stakeholders and building owners. In particular, the proposed framework is utilized to compute the disaggregated losses if the same buildings were to be retrofitted prior to the same seismic event. In particular, if the beam-to-column connections would be rehabilitated such that they could behave as standard post-Northridge beam-to-column connections then the expected losses due to moment connection repairs would be nearly zero as shown in Figure 17(c). Similarly, the

expected losses due partition repairs would be reduced by a factor of 2.5, on average, if sliding gypsum wallboard partitions would be installed prior to the seismic event.

4. Limitations of the proposed framework

This paper proposes a nonmodel-based framework for the rapid seismic risk and loss assessment of instrumented steel frame buildings. The potential applicability of this framework for city-scale risk assessment is also investigated. This section summarizes limitations of the proposed framework that can provide the basis for further research. In particular, the proposed framework can only provide information in a global sense. The exact location of structural damage within a story is not possible to be traced. The examined instrumented steel frame buildings were all fairly symmetric and therefore torsional effects were not deemed to be critical. This issue should be further investigated. The relationship between story-based EDPs and wavelet-based damage sensitive features should be defined for other lateral load resisting systems such as concentrically braced frames as well as shear wall structures. Furthermore, soil-foundation-structure interaction (SFSI) effects were not considered. Prior studies on SFSI effects suggest that their influence on story-based EDP demands may be appreciable depending on the soil type [75–77]. This issue deserves more attention in future research studies.

5. Summary and conclusions

This paper proposes a nonmodel-based framework for rapid seismic risk and loss assessment of instrumented steel frame buildings in the aftermath of an earthquake. The proposed framework utilizes a wavelet-based damage-sensitive feature (DSF) and minimal information to infer the damage state of a building at a given seismic intensity. The wavelet-based DSF is able to trace the changes in the building's seismic response as verified with experimental data from shake table experiments. The proposed framework predicts with relatively good accuracy story-based engineering demand parameters (EDPs) that are typically used within a performance-based earthquake engineering framework for building specific earthquake-induced loss assessment. In particular, story-based EDPs of interest include the peak story drift ratios (SDRs), residual SDRs and peak floor absolute accelerations (PFAs) along the height of a building.

The efficiency and potential of the proposed framework in computing story-based EDPs at a given seismic intensity is evaluated through a number of illustrative applications including code-compliant archetype buildings with MRFs. It is found that the nonmodel-based framework provides better estimates of peak SDRs and PFAs regardless of the seismic intensity of interest compared to the FEMA P-58 simplified approach that utilizes a detailed numerical model representation of the building of interest. Although the proposed framework predicts reasonably well the residual SDRs for moderate seismic events, large discrepancies are observed between predicted and simulated median residual SDRs at seismic intensities with low probability of occurrence. In this case, lower/upper bound analysis should be considered.

The potential use of the proposed framework for rapid seismic risk and loss assessment at a city-scale is illustrated with a grid of instrumented steel frame buildings that experienced the 1994 Northridge earthquake through the development of so-called generalized damage and loss maps. These maps are generated with the geographic information system (GIS) and can be available within minutes after the seismic event. The same maps suggest that the primary contributors to the expected losses in the instrumented buildings were the repairs due to premature fracture of pre-Northridge beam-to-column connections and the repairs due to conventional gypsum wallboard partition damage. The proposed nonmodel based framework is utilized to examine the efficiency of a retrofit scenario in which pre-Northridge beam-to-column connections and wallboard partitions were upgraded to meet today's seismic performance standards. It is shown that the proposed framework can effectively serve for pre-disaster risk management. Summary remarks on how to improve the proposed framework are also provided.

Acknowledgement

This study is based on work supported by the Fonds de recherché du Québec – Nature et technologies, Projet de Recherché en Equipe, Award No. FQRNT 2013-PR-167747. Financial support was also provided by the Swiss Federal Institute of Technology in Lausanne (EPFL). The financial support is gratefully acknowledged. The authors would like to sincerely thank Dr. Ahmed Elkady for sharing his nonlinear steel moment-resisting frame building simulation results. The authors also thank Dr. Tsuyoshi Hikino and Prof. Masayoshi Nakashima for providing the experimental data of the 4-story steel building tested at the E-Defense facility administered by the National Research Institute for Earth Science and Earthquake Mitigation (NIED). Any opinions, findings, and conclusions or recommendations expressed in this paper are those of the authors and do not necessarily reflect the views of the sponsors.

References

[1] FEMA, Rapid Visual Screening of Buildings for Potential Seismic Hazards: a handbook, Technical Report No. FEMA P-155, prepared by Applied Technology Council for the Federal Emergency Management Agency, Washington, DC, 2015.

[2] NRCC, Manual for Screening of Buildings for Seismic Investigation, Institute for Research in Construction, National Research Council of Canada, Ottawa, ON, Canada, 1992.

[3] JPDPA, Seismic Evaluation and Retrofit, Japan Building Disaster Prevention Association, Tokyo, Japan, 2001.

[4] NZSEE, Assessment and Improvement of the Structural Performance of Buildings in Earthquakes, Recommendations of a NZSEE Study Group on Earthquake Risk Buildings, New Zealand Society for Earthquake Engineering, Wellington, New Zealand, 2006.

[5] O. C. Celik, B. R. Ellingwood, Seismic fragilities for non-ductile reinforced concrete frames – role of aleatoric and epistemic uncertainties, Structural Safety 32 (2010) 1–12.

[6] J.-S. Jeon, J.-H. Park, R. DesRoches, Seismic fragility of lightly reinforced concrete frames with masonry infills, Earthquake Engineering & Structural Dynamics 44 (2015) 1783–803.

[7] C.-L. Lee, R. K. L. Su, Fragility analysis of low-rise masonry in-filled reinforced concrete buildings by a coefficient-based spectral acceleration method, Earthquake Engineering & Structural Dynamics 41 (2012) 697–713.

[8] J. Erochko, C. Christopoulos, R. Tremblay, H. Choi, Residual drift response of SMRFs and BRB frames in steel buildings designed according to ASCE 7-05, Journal of Structural Engineering 137 (2011) 589–99.

[9] FEMA, Seismic performance assessment of buildings, Volume 1-Methodology, Technical Report No. FEMA P-58-1, prepared by the Applied Technology Council for the Federal Emergency Management Agency, Washington, DC, 2012.

[10] J. Ruiz-García, C. Chora, Evaluation of approximate methods to estimate residual drift demands in steel framed buildings, Earthquake Engineering & Structural Dynamics 44 (2015) 2837–54.

[11] J. Ruiz-García, E. Miranda, Probabilistic estimation of residual drift demands for seismic assessment of multi-story framed buildings, Engineering Structures 32 (2010) 11–20.

[12] X. Ji, G. L. Fenves, K. Kajiwara, M. Nakashima, Seismic damage detection of a full-scale shaking table test structure, Journal of Structural Engineering 137 (2011) 14–21.

[13] B. Moaveni, X. He, J. P. Conte, J. I. Restrepo, M. Panagiotou, System identification study of a 7-story full-scale building slice tested on the UCSD-NEES shake table, Journal of Structural Engineering 137 (2011) 705–17.

[14] S. N. Pakzad, G. L. Fenves, Statistical analysis of vibration modes of a suspension bridge using spatially dense wireless sensor network, Journal of Structural Engineering 135 (2009) 863–72.

[15] J. Kim, J. P. Lynch, Subspace system identification of support-excited structures–part I: theory and black-box system identification, Earthquake Engineering & Structural Dynamics 41 (2012) 2235–51.

[16] J. Goulet, C. Michel, A. D. Kiureghian, Data-driven post-earthquake rapid structural safety assessment, Earthquake Engineering & Structural Dynamics 44 (2015) 549–62.

[17] H. Y. Noh, K. K. Nair, D. G. Lignos, A. S. Kiremidjian, Use of wavelet-based damage-sensitive features for structural damage diagnosis using strong motion data, Journal of Structural Engineering 137 (2011) 1215–28.

[18] H. Y. Noh, D. G. Lignos, K. K. Nair, A. S. Kiremidjian, Development of fragility functions as a damage classification/prediction method for steel moment-resisting frames using a wavelet-based damage sensitive feature, Earthquake Engineering & Structural Dynamics 41 (2012) 681–96.

[19] M. Çelebi, Seismic monitoring of structures and new developments, chapter 2, in: M. Garevski (Ed.), Earthquakes and Health Monitoring of Civil Structures, Springer Netherlands, Dordrecht, 2013, pp. 37–84.

[20] T. Kashima, S. Koyama, I. Okawa, M. Iiba, Strong motion records in buildings from the 2011 Great East Japan earthquake, in: Proceedings of the 15th World Conference on Earthquake Engineering (15WCEE), Lisbon, Portugal, 2012, p. 1768.

[21] E. M. Thomson, B. A. Bradley, Preliminary analysis of instrumented Wellington building responses in the July/August 2013 Seddon/Lake Grassmere earthquakes, in: Proceedings of the 2014 New Zealand Society of Earthquake Engineering (NZSEE) Conference, Auckland, New Zealand, 2014, p. 48.

[22] X. Li, M. Kurata, A. Suzuki, Decoupling algorithm for evaluating multiple beam damages in steel moment-resisting frames, Earthquake Engineering & Structural Dynamics (2016). (in press).

[23] G. Simkin, S. Beskhyroun, Q. Ma, L. Wotherspoon, J. Ingham, Measured response of instrumented buildings during the 2013 Cook strait earthquake sequence, Bulletin of the New Zealnd for Earthquake Engineering (2015) 223–34.

[24] S.-H. Hwang, D. G. Lignos, Assessment of structural damage detection methods for steel structures using full-scale experimental data and nonlinear analysis, Bulletin of Earthquake Engineering (2017). (under review).

[25] A. V. Oppenheim, R. W. Schafer, J. R. Buck, Discrete-Time Signal Processing, 2nd ed., Prentice Hall, Upper Saddle River, NJ, 1999.

[26] K. Suita, S. Yamada, M. Tada, K. Kasai, Y. Matsuoka, Y. Shimada, Collapse experiment of 4-story steel moment frame: part 2 detail of collapse behavior, in: Proceedings of the 14th World Conference on Earthquake Engineering (14WCEE), Beijing, China, 2008, p. 011.

[27] S. Yamada, K. Suita, M. Tada, K. Kasai, Y. Matsuoka, Y. Shimada, Collapse experiment of 4-story steel moment frame: part 1 outline of test of results, in: Proceedings of the 14th World Conference on Earthquake Engineering (14WCEE), Beijing, China, 2008, p. 004.

[28] J. Morlet, G. Arens, E. Fourgeau, D. Glard, Wave propagation and sampling theory–part I: Complex signal and scattering in multilayered media, Geophysics 47 (1982) 203–21.

[29] A. K. Chopra, Dynamics of structures: Theory and applications to earthquake engineering, 4th ed., Prentice Hall, Upper Saddle River, NJ, 2011.

[30] AISC, Seismic provisions for structural steel buildings, ANSI/AISC 341-10, American Institute of Steel Construction, Chicago, IL, 2010.
[31] ASCE, Minimum design loads for buildings and other structures, ASCE/SEI 7-10, American Society of Civil Engineers, Reston, VA, 2010.
[32] A. Elkady, D. G. Lignos, Effect of composite action on the dynamic stability of special steel moment resisting frames designed in seismic regions, in: Proceedings of ASCE Structures Congress 2013, Pittsburgh, PA, 2013, pp. 2151–60.
[33] A. Elkady, D. G. Lignos, Modeling of the composite action in fully restrained beam-to-column connections: implications in the seismic design and collapse capacity of steel special moment frames, Earthquake Engineering & Structural Dynamics 43 (2014) 1935–54.
[34] A. Elkady, D. G. Lignos, Effect of gravity framing on the overstrength and collapse capacity of steel frame buildings with perimeter special moment frames, Earthquake Engineering & Structural Dynamics 44 (2015) 1289–307.
[35] F. T. McKenna, Object oriented finite element programming frameworks for analysis, algorithms and parallel computings, Ph.D. thesis, University of California at Berkeley, Berkeley, CA, 1997.
[36] L. F. Ibarra, R. A. Medina, H. Krawinkler, Hysteretic models that incorporate strength and stiffness deterioration, Earthquake Engineering & Structural Dynamics 34 (2005) 1489–511.
[37] D. G. Lignos, F. Zareian, H. Krawinkler, A steel component database for deterioration modeling of steel beams with RBS under cyclic loading, in: Proceedings of ASCE Structures Congress 2010, Orlando, FL, 2010, pp. 1241–52.
[38] D. G. Lignos, H. Krawinkler, Deterioration modeling of steel components in support of collapse prediction of steel moment frames under earthquake loading, Journal of Structural Engineering 137 (2011) 1291–302.
[39] C. Gilton, B. Chi, C.-M. Uang, Cyclic response of RBS moment connections: weak-axis configuration and deep column effects, Technical Report No. SSRP-99/21, Department of Structural Engineering, University of California, San Diego, La Jolla, CA, 2000.
[40] A. Gupta, H. Krawinkler, Seismic demands for the performance evaluation of steel moment resisting frame structures, Technical Report No. 132, The John A. Blume Earthquake Engineering Center, Stanford University, Stanford, CA., 1999.
[41] D. Vamvatsikos, C. A. Cornell, Incremental dynamic analysis, Earthquake Engineering & Structural Dynamics 31 (2002) 491–514.
[42] R. A. Medina, H. Krawinkler, Seismic demands for nondeteriorating frame structures and their dependence on ground motions, Technical Report No. 144, The John A. Blume Earthquake Engineering Center, Stanford University, Stanford, CA, 2003.
[43] S. Chatterjee, A. S. Hadi, Regression analysis by example, 5th ed., John Wiley & Sons Inc., New York, NY, 2012.
[44] P. P. Cordova, G. G. Deierlein, S. S. Mehanny, C. Cornell, Development of a two-parameter seismic intensity measure and probabilistic assessment procedure, in: Proceedings of the 2nd US-Japan Workshop on Performance-based Earthquake Engineering Methodology for RC Building Structures, Sapporo, Japan, 2000.
[45] E. Bojórquez, I. Iervolino, Spectral shape proxies and nonlinear structural response, Soil Dynamics and Earthquake Engineering 31 (2011) 996–1008.
[46] L. Eads, E. Miranda, D. G. Lignos, Average spectral acceleration as an intensity measure for collapse risk assessment, Earthquake Engineering & Structural Dynamics 44 (2015) 2057–73.
[47] A. Arias, A measure of earthquake intensity, in: R. Hansen (Ed.), Seismic design for nuclear power plants, MIT Press, Cambridge, MA, 1970, pp. 438–?483.
[48] L. Eads, E. Miranda, D. G. Lignos, Spectral shape metrics and structural collapse potential, Earthquake Engineering & Structural Dynamics 45 (2016) 1643–59.
[49] D. G. Lignos, E. Miranda, Estimation of base motion in instrumented steel buildings using output-only system identification, Earthquake Engineering & Structural Dynamics 43 (2014) 547–63.
[50] C. Christopoulos, S. Pampanin, M. J. N. Priestley, Performance-based seismic response of frame structures including residual deformations part I: Single-degree of freedom systems, Journal of Earthquake Engineering 7 (2003) 97–118.
[51] S. Pampanin, C. Christopoulos, M. J. N. Priestley, Performance-based seismic response of frame structures including residual deformations. part II: Multi-degree of freedom systems, Journal of Earthquake Engineering 7 (2003) 119–47.
[52] J. Ruiz-García, E. Miranda, Residual displacement ratios for assessment of existing structures, Earthquake Engineering & Structural Dynamics 35 (2006) 315–36.

[53] G. A. MacRae, K. Kawashima, Post-earthquake residual displacement of bilinear oscillators, Earthquake Engineering & Structural Dynamics 26 (1997) 701–16.

[54] S.-H. Hwang, D. G. Lignos, Earthquake-induced loss assessment of steel frame buildings with special moment frames designed in highly seismic regions, Earthquake Engineering & Structural Dynamics 46 (2017) 2141–62.

[55] FEMA, Quantification of building seismic performance factors, Technical Report No. EMA-P695, Federal Emergency Management Agency, Washington, DC, 2009.

[56] S.-H. Hwang, A. Elkady, S. Al.Bardaweel, D. G. Lignos, Earhtuqake loss assessment of steel frame buildings desinged in highly seismic regions, in: Proceedings of the 5th ECCOMAS Thematic Conference on Computational Methods in Structural Dynamics and Earthquake Engineering, Crete Island, Greece, 2015, pp. 1496–512.

[57] S.-H. Hwang, A. Elkady, D. G. Lignos, Design decision support for steel frame buildings through an earthquake-induced loss assessment, in: Proceedings of ATC-SEI 2nd Conference on Improving the Seismic Performance of Existing Buildings and Other Structures, San Francisco, CA, 2015, pp. 340–52.

[58] C. M. Hutt, I. Almufti, M. Willford, G. G. Deierlein, Seismic loss and downtime assessment of existing tall steel-framed buildings and strategies for increased resilience, Journal of Structural Engineering 142 (2016) C4015005–1.

[59] C. M. Ramirez, E. Miranda, Significance of residual drifts in building earthquake loss estimation, Earthquake Engineering & Structural Dynamics 41 (2012) 1477–93.

[60] R. Villaverde, Seismic analysis and design of nonstructural elements, chapter 19, in: Y. Bozorgnia, V. V. Bertero (Eds.), Earthquake engineering: from engineering seismology to performance-based engineering, CRC press, Boca Raton, FL, 2004, pp. 19–1 to 19.

[61] S. Soroushian, E. Rahmanishamsi, K. P. Ryu, M. Maragakis, A. M. Reinhorn, Experimental fragility analysis of suspension ceiling systems, Earthquake Spectra 32 (2016) 881–908.

[62] C. M. Ramirez, D. G. Lignos, E. Miranda, Fragility functions for pre-Northridge welded steel moment-resisting beam-to-column connections, Engineering Structures 45 (2012) 574–84.

[63] G. Araya-Letelier, E. Miranda, Novel sliding/frictional connections for improved seismic performance of gypsum wallboard partitions, in: Proceedings of the 15th World Conference on Earthquake Engineering (15WCEE), Lisbon, Portugal, 2012, p. 4409.

[64] C. M. Ramirez, A. B. Liel, J. Mitrani-Reiser, C. B. Haselton, A. D. Spear, J. Steiner, G. G. Deierlein, E. Miranda, Expected earthquake damage and repair costs in reinforced concrete frame buildings, Earthquake Engineering & Structural Dynamics 41 (2012) 1455–75.

[65] B. A. Bradley, R. P. Dhakal, M. Cubrinovski, G. A. MacRae, D. S. Lee, Seismic loss estimation for efficient decision making, Bulletin of the New Zealand Society of Earthquake Engineering 42 (2009) 96–110.

[66] J. Mitrani-Reiser, An ounce of prevention: probabilistic loss estimation for performance-based earthquake engineering, Ph.D. thesis, California Institute of Technology, Pasadena, CA, 2007.

[67] D. G. Lignos, D. Kolios, E. Miranda, Fragility assessment of reduced beam section moment connections, Journal of Structural Engineering 136 (2010) 1140–50.

[68] C. W. Roeder, State of the art report on connection performance, Technical Report No. FEMA-355D, Federal Emergency Management Agency, Washington, DC, 2000.

[69] E. Miranda, C. J. Reyes, Approximate lateral drift demands in multistory buildings with nonuniform stiffness, Journal of Structural Engineering 128 (2002) 840–9.

[70] E. Miranda, S. Taghavi, Approximate floor acceleration demands in multistory buildings. I: Formulation, Journal of Structural Engineering 131 (2005) 203–11.

[71] M. Ervasti, S. Dashti, J. Reilly, J. D. Bray, A. Bayen, S. Glaser, iShake: mobile phones as seismic sensors – user study findings, in: Proceedings of the 10th International Conference on Mobile and Ubiquitous Multimedia, Beijing, China, 2011, pp. 43–52.

[72] M. Faulkner, M. Olson, R. Chandy, J. Krause, K. M. Chandy, A. Krause, The next big one: Detecting earthquakes and other rare events from community-based sensors, in: Proceedings of the 10th ACM/IEEE International Conference on Information Processing in Sensor Networks, Chicago, IL, 2011, pp. 13–24.

[73] ArcGIS, ArcGIS release version 10.3, Environmental Systems Research Institute (ESRI), Redlands, CA, 2014.

[74] P. M. Bartier, C. Keller, Multivariate interpolation to incorporate thematic surface data using inverse distance weighting (IDW), Computers & Geosciences 22 (1996) 795 –9.

[75] M. J. Givens, J. P. Stewart, C. B. Haselton, S. Mazzoni, Assessment of soil-structure interaction modeling strategies for response history analysis of buildings, in: Proceedings of the 15th World Conference on Earthquake Engineering (15WCEE), Lisbon, Portugal, 2012, p. 5552.

[76] NIST, Soil-structure interaction for building structures, Technical Report No. NIST GCR 12-917-21, prepared by the NEHRP Consultants Joint Venture for the National Institute of Standards and Technology, Gaithersburg, MD, 2012.

[77] L. B. Storie, M. J. Pender, G. C. Clifton, L. M. Wotherspoon, Soil-foundation-structure interaction for buildings on shallow foundations in the Christchurch earthquake, in: Proceedings of the tenth U.S. National Conference on Earthquake Engineering Frontiers of Earthquake Engineering (10NCEE), Anchorage, AK, 2014, p. 1259.